Hindawi Publishing Corporation
Advances in Mechanical Engineering
Volume 2013, Article ID 421681, 17 pages
http://dx.doi.org/10.1155/2013/421681

Research Article

Comparison of Heat Insulations for Cryogenic Tankers Using Analytical and Numerical Analysis

Ramón Miralbés Buil[1] and David Valladares Hernando[2]

[1] *Department of Design and Manufacturing, University of Zaragoza, 50017 Zaragoza, Spain*
[2] *Department of Mechanical Engineering, University of Zaragoza, 50017 Zaragoza, Spain*

Correspondence should be addressed to Ramón Miralbés Buil; miralbes@unizar.es

Received 15 May 2013; Accepted 26 June 2013

Academic Editor: Magd Abdel Wahab

This paper presented a methodology for the design of heat insulations used in cryogenic tankers. This insulation usually comprises a combination of vacuum and perlite or vacuum and superinsulation. Concretely, it is a methodology to obtain the temperatures, heat fluxes, and so forth. Using analytical tools has been established, which is based on the equivalence with an electric circuit, and on numerical tools using finite elements. Results obtained with both methods are then compared. In addition, the influence of the outer finish of the external part, due to the effect of the solar radiation, is analyzed too, and the equations to determine the maximum time available to transport the cryogenic liquid have been established. All these aspects are applied to a specific cryogenic commercial vehicle.

1. Introduction

A main aspect of any type of cryogenic device is the heat insulation of its content. The case of a cryogenic tanker for liquefied gases is not an exception so during the design stages, it is necessary to carry out a detailed study and analysis of the thermic phenomena that take place during the use of the tanker. It is also necessary a thermic analysis to choose and to dimension correctly the insulation used in the zones between the two main parts of the tanker so as to reduce the heat flux, with the resulting heating of the load, and to allow a higher storage time [1]; this aspect involves that the vehicle has a higher range distance. On the other hand, if heat losses are reduced, the energy needed in the discharge point to cool the gas is lower and appears an energy benefit [2].

Nowadays, the thermic analysis that some vehicle designers of the main manufacturing companies make has a low precision and is based on some coarse simplifications of the problem, so the results have low precision [3].

This paper explains some techniques to make a thermal analysis of these types of vehicles, using analytical and numerical tools.

The main thermal insulation methods used in the cryogenic industry [4, 5] are based on the combination of vacuum and superinsulation (based on the Dewar flask) and vacuum with expanded perlite. The use of one or another technique depends on some aspects: economical, manufacturing, gas transported, and so forth.

Another aspect analyzed is the maximum range time to make the transport, depending on some aspects like the weather, wind, external temperature, filling grade, and so forth. All these aspects are dealt theoretically and applied to a commercial cryogenic tanker.

2. Heat Transmission Methods

There are three different heat transmission mechanisms: conduction, convection, and radiation.

2.1. Conduction. Conduction is the energy transmission method based on the transmission of the energy between adjacent molecules; it is the heat transmission method of the solids and has not influence in the other states of the material

(liquid and gas). The Fourier law (see (1)) with the thermal conductivity constant (k) defines it [6] as follows:

$$q''_{\text{cond}} = k\Delta T. \tag{1}$$

2.2. Convection. It appears in the liquids and in the gases, and it is due to the particle movement associated with the variation of its temperature and its density.

This phenomenon depends on the fluid characteristics; if the fluid has a movement related to the tanker, then a forced convection appears, and in an other case a natural convection occurs. Both can be laminar or turbulent, depending on the Reynolds number (Re).

In this case, the convection transmission appears only in the exterior surface of the outer main part of the tanker, and (2), with the thermal convection coefficient (h_c), defines it [6] as follows:

$$q''_{\text{conv}} = \frac{\Delta T}{h_c}. \tag{2}$$

Before the beginning of the calculation of the convection coefficient, the Nusselt number (Nu_m) must be introduced; it relates the convection flux with the conduction flux in a fluid [6]:

$$\text{Nu}_m = \frac{h_c \cdot L_c}{k}, \tag{3}$$

where L_c is the characteristic length that for this case is the total length of the vehicle. In this case, the natural convection is quite difficult to obtain using experimental and theoretical tools, but it can be approximated as the natural convection of a horizontal cylinder with a diameter D, so (4) and (5) are obtained [6] as follows:

$$\text{Nu}_m = \frac{4}{3} \cdot f(\text{Pr}) \cdot \left(\frac{\text{Gr}_D}{4}\right)^{1/4} = \frac{h_c \cdot D}{k}, \tag{4}$$

$$\text{Gr}_d = \frac{g \cdot (T_{\text{ext}} - T_{\text{env}}) \cdot D^3}{\nu^2_{\text{air}}}, \tag{5}$$

where Pr is the Prandtl number Gr_d is the Grashoff number, g is the gravity, T_{env} is the environmental temperature and T_{ext} is the temperature of the exterior surface. The main problem of these equations is that Gr_d depends on T_{ext}, which is an unknown factor, so it must be estimated initially. The real value can be obtained later using iterative calculus.

For the forced convection, the Nusselt number can be obtained using [6] and the obtained values for the study case is show in Table 1

$$\text{Nu}_m = 0.664 \cdot \text{Re}_l^{1/2} \cdot \text{Pr}^{1/3} \quad \text{for} \quad \text{Re} \le 5 \cdot 10^5, \tag{6}$$

$$\text{Nu}_m = \left(0.037 \cdot \text{Re}^{0.8} - 872\right) \cdot \text{Pr}^{1/3} \quad \text{for others}, \tag{7}$$

where Re is the Reynolds number:

$$\text{Re} = \frac{V_\infty \cdot L}{\nu}, \tag{8}$$

where V_∞ is the relative velocity between the tanker and the environment and L is the length of the vehicle.

In this particular case, it can be observed that, after the tractor cabin, the flow become into a turbulent one, so (7) is going to be used in this methodology.

2.3. Radiation. It is an energy transmission phenomenon that occurs because a material has a temperature and emits electromagnetic waves. As the light, the emitted heat can be reflected, refracted, and absorbed. In this case there are some different elements that emit radiation: the environment, the sun, the different parts of the tanker, and so forth.

The radiation can be defined using the Steffan-Bolzman equation [6]:

$$q''_{\text{rad}} = \varepsilon\sigma T^4_{\text{sup}}, \tag{9}$$

where ε is the emissivity coefficient and σ is the Stefan-Boltzmann one ($5.67 \cdot 10^8$ W/m^2 K^4).

In this case, the radiation for the exterior part of the tanker can be obtained doing an energy balance (Figure 1).

2.3.1. Incident Radiation

(i) Solar incident radiation (G): depending of some aspects such as the climatology and the geographic situation, varying between 0 and 1000 W/m^2.

(ii) Environmental radiation (H): due to the effect of the environmental gases. The value of the environmental emissivity (ε_a) can be obtained using the Verdal and Fromberg equations [6]:

$$\varepsilon_{a,\text{day}} = 0.741 + 0.0063T_{dp}\,(^\circ\text{C}), \tag{10}$$

$$\varepsilon_{a,\text{night}} = 0.727 + 0.0060T_{dp}\,(^\circ\text{C}), \tag{11}$$

where $T_{dp} = T_a + \log(H_r)$, and T_a is the dew temperature and H_r is the relative humidity.

2.3.2. Emitted Radiation. It is due to the reflected radiation (J), where α is the absorption coefficient of the exterior part of the tanker, $\varepsilon \approx \alpha$ is the emission coefficient, and α_S is the solar absorption coefficient of the exterior of the tanker, and depends on the material, color, and exterior temperature.

2.3.3. Absorbed Radiation. After doing an equation balance, (12) is obtained:

$$q''_{\text{rad,abs}} = \alpha_{\text{sext}}\left(G + \varepsilon_a\sigma T_a^4\right) - \varepsilon_{\text{ce}}\sigma T^4_{\text{ce}}. \tag{12}$$

Additionally the solar radiation (G) occurs only in a specific zone of the tanker and so, for the axisymmetric and for the theoretical case, it must be modified using

$$G_{\text{axi-teo}} = G \cdot \frac{A_{\text{ext\_pro}}}{A_{\text{ext}}}. \tag{13}$$

Table 1: Nusselt numbers and convection coefficient for the thermic cases to study.

T_{amb} (°C)	V_{amb} (Km/h)	Re	Pr	Nu_m	h_c (W/m^2·K)
−10.00	100.00	36500000	0.72	36384.43	65.21
	200.00	73000000	0.72	63927.72	114.58
0.00	100.00	34000000	0.72	34289.91	63.30
	200.00	68000000	0.72	60280.22	111.29
20.00	100.00	27000000	0.70	28189.87	57.03
	200.00	54000000	0.70	49655.49	100.46
50.00	100.00	24000000	0.70	25603.52	55.34
	200.00	48000000	0.70	45152.81	97.60

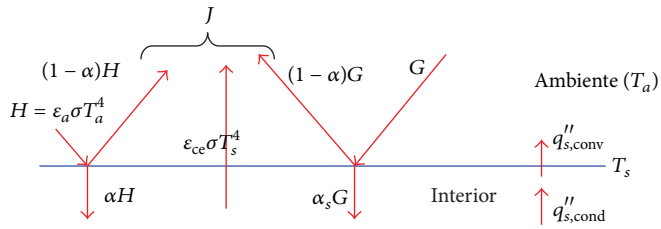

Figure 1: Energy balance for the exterior part of the tanker.

3. The Thermic Insulation

There are two different insulation configurations.

3.1. Perlite Insulation. Perlite is the name of a natural silicate that has a 65–75% of SiO_2, a 10–20% of Al_2O_3, and a 2–5% of water. To be used industrially, it must be subjected to an expansion process, where it is heated until 1000°C; in this process, water evaporates, the material internal structure is modified and perlite increases 20 times its volume, becoming into expanded perlite.

The main advantages are that it is a natural material, it has not toxic emissions, it is chemically neutral (pH 7), it is fire resistant, and it is the cheapest industrial insulation.

Perlite thermal properties depend on its density and its grain size. For cryogenic applications the common density is between 128 and 152 Kg/m^3 (see Figure 2).

Usually cryogenic tankers use expanded perlite inside and with a high degree of vacuum (until 100 Hg mm) it is obtained a low conductivity. Thus, the radiation flux between the interior and the exterior parts of the tanker disappears.

The use of vacuum with this material implies a decrease of the density and the conductivity. For cryogenic tankers, a common value of the density is 4 Kg/m^3 and, as a result of this, conductivity is 22 times lower than the value corresponding to the material with density 139 Kg/m^3.

The main disadvantage of perlite usually tends to compact in the bottom zone of the tanker, producing as a result a nonuniform insulation.

3.2. Insulation Using "Superinsulation". This insulation method is based on the Dewar balloon. In cryogenic tankers, a vacuum is created inside the tanker using a pump; in this way the convection flux is avoided, but not the radiation flux.

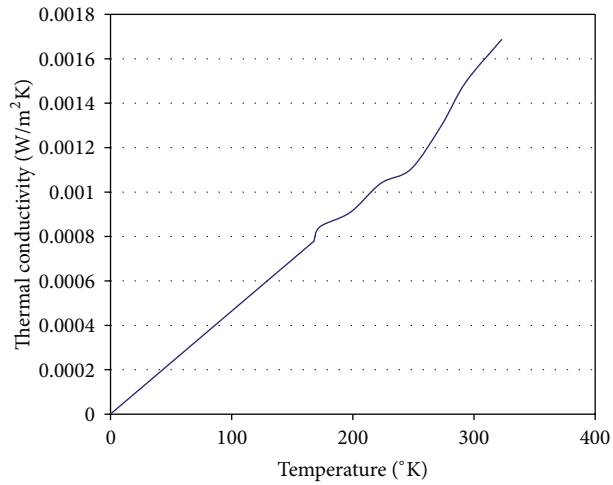

Figure 2: Conductivity values for perlite with grain size 1 m and density 4 Kg/m^3.

In a cryogenic tanker, there is usually a material called "multilayer insulation" (MLI) to reduce the radiation. This material is made of some small layers and acts like a radiation shield. These layers must be separated between themselves to avoid the conduction, so usually there are some nylon and polystyrene inner layers.

Usually, 60 layers per inch multilayers are used [7], but the radiation insulation depends not only on the thickness of the multilayer but also on the vacuum grade. Figure 3 shows the equivalent conductivity for this insulation system [8].

The main disadvantages of the multilayer insulation appear because it is difficult to use it at complex geometries, and it is sensitive to the mechanical compression effects and must be manufactured carefully.

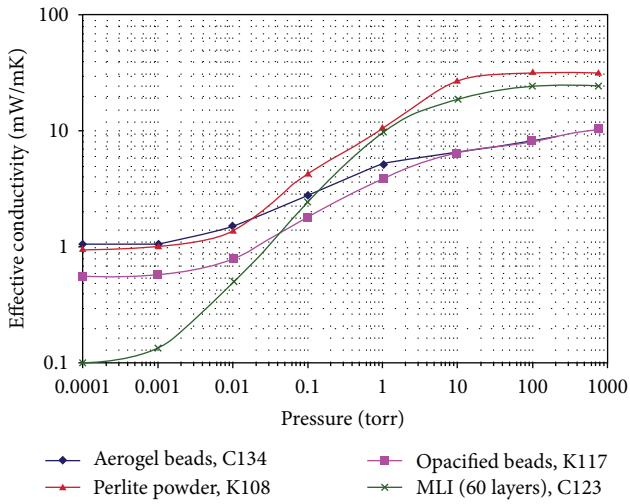

Figure 3: Effective conductivity for several insulation materials.

For the application of this insulation system in cryogenic tankers, a composite combination of multilayer (5 mm/layer) and rock wool (20 mm/layer) [7] is made. Usually a five-layer configuration (see Figure 4) is used.

This composite configuration is used because the multilayer material is quite expensive, and in this way the final cost is reduced.

Nowadays there are two different configurations, depending on the zone of the tanker where it is fixed: in the exterior or in the interior part. These configurations imply that exist a free zone between the end of the insulation and the other part of the tanker and so appears some radiation phenomena that must be taken into account. There appear some reflection and absorption effects, as can be seen in Figure 5.

By means of an energy balance, the heat flux is obtained:

$$q''_{\mathrm{rad,ext}} = \varepsilon_{\mathrm{ext}}\sigma T_{\mathrm{ext}}^4 - \varepsilon_{\mathrm{ext}}\sigma T_{\mathrm{ext}}^4\alpha_{\mathrm{ext}}\sum_{i=0}^{\infty}\left[(1-\alpha_{\mathrm{int}})^{i+1}(1-\alpha_{\mathrm{ext}})^{i}\right] - \varepsilon_{\mathrm{int}}\sigma T_{\mathrm{int}}^4\alpha_{\mathrm{int}}\frac{A_{\mathrm{int}}}{A_{\mathrm{ext}}}\sum_{i=0}^{\infty}\left[(1-\alpha_{\mathrm{ext}})^{i}(1-\alpha_{\mathrm{int}})^{i}\right],$$

$$q''_{\mathrm{rad,int}} = \varepsilon_{\mathrm{int}}\sigma T_{\mathrm{int}}^4 - \varepsilon_{\mathrm{int}}\sigma T_{\mathrm{int}}^4\alpha_{\mathrm{int}}\sum_{i=0}^{\infty}\left[(1-\alpha_{\mathrm{ext}})^{i+1}(1-\alpha_{\mathrm{int}})^{i}\right] - \varepsilon_{\mathrm{ext}}\sigma T_{\mathrm{ext}}^4\alpha_{\mathrm{ext}}\frac{A_{\mathrm{int}}}{A_{\mathrm{ext}}}\sum_{i=0}^{\infty}\left[(1-\alpha_{\mathrm{ext}})^{i}(1-\alpha_{\mathrm{int}})^{i}\right]. \quad (14)$$

4. Thermal Load Cases

In the thermal analysis of the tanker, depending on the boundaries considered, different load cases can be analysed. The boundaries to study are as follos.

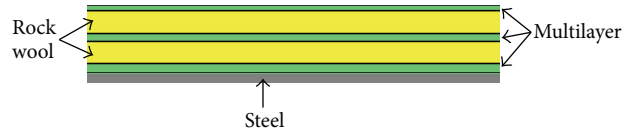

Figure 4: Multilayer with rock wool insulation.

(i) Relative air velocity: it is due to the movement of the vehicle and the movement of the air and can appear superposed, so then the equivalent velocity is the addition of both. It has been considered a velocity for the vehicle and for the wind between 0 and 100 Km/h [9]. As a result of this three different velocities will be studied: 0, 100, and 200 Km/h.

(ii) Exterior temperature: there have been studied four different temperatures: −10, 0, 20, and 50°C.

(iii) Radiation (G): there have been studied three different solar radiation cases: without sun (0 W/m^2), average radiation (500 W/m^2), and extreme radiation (1000 W/m^2) [10].

All in all there are thirty-six different load cases for each insulation configuration; there are two extreme load cases:

(i) maximum energy profit: 200 Km/h air velocity, G = 1000 W/m^2 K, and 50°C air temperature

(ii) minimum energy profit: 0 Km/h air velocity, G = 0 W/m^2 K, and −10°C air temperature.

5. Analytical Calculation of the Insulation

The thermal analytical calculus is governed by the following differential equation:

$$\nabla\cdot(k\nabla T) + \dot{q} = \rho c\frac{\partial T}{\partial t}. \quad (15)$$

If the stationary state is analyzed and there is not heat generation inside the tanker, the equation becomes into this one:

$$\nabla^2 T = 0. \quad (16)$$

This equation has analytical solutions for simple geometries [10]: cylinders, spheres, shells,... but not for this particular case, so it cannot be solved exactly.

Due to this fact, an approximated analytical calculus must be made, and the tanker must be considered as a complex geometry comprising two cylinders, one inside the other, and four spherical caps.

In this calculus, there have been taken into account the insulation and the steel parts of the different joint zones.

5.1. Analytical Calculation with Perlite. In this case the tanker can be approximated with the equivalent electric circuit (Figure 6).

After the definition of the equivalent circuit, the different variables involved must be obtained.

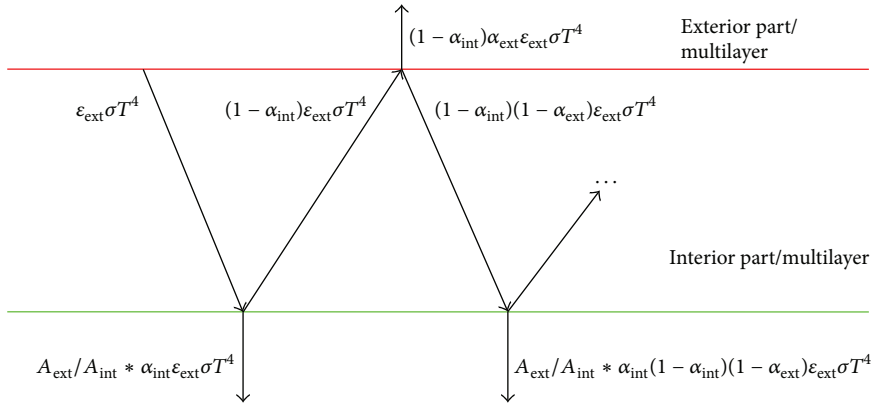

Figure 5: Radiation balance between the multilayer and the corresponding part.

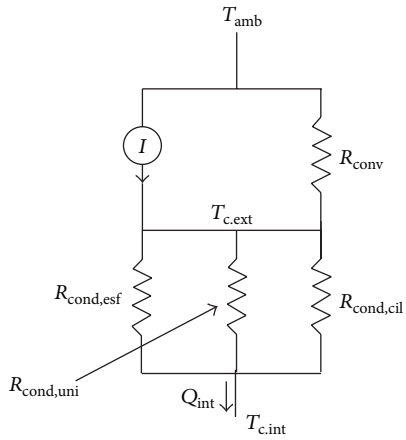

Figure 6: Equivalent circuit for the perlite insulation configuration.

(i) I is the power due to the radiation emissions. It can be obtained using this equation that is obtained doing the energy balance of the Figure 5:

$$I = A_{ext} \cdot q''_{rad,abs} = \left(2\pi r_{ext} l_{cyl} + 4\pi r_{ext}^2\right) q''_{rad,abs}, \quad (17)$$

where $q''_{rad,abs}$ is obtained from (13).

(ii) R_{conv} is the thermal resistance due to the air convention, and their equation is

$$R_{conv} = \frac{1}{h_{conv} A_{ext}}, \quad (18)$$

where h_{conv} is obtained using (4), (6) and (7).

(iii) $R_{cond,esp}$ is the thermal resistance due to the conduction in the spherical zones and is defined in the following equation:

$$R_{cond,esp} = \frac{1/r_{int} - 1/r_{ext}}{4\pi k_{perlite}}, \quad (19)$$

where $k_{perlite}$ depends on the temperature, so for this case the conductivity will be used at the average temperature: $(T_{amb} + T_{int})/2$.

(iv) $R_{cond,cyl}$ is the thermal resistance for the cylindrical zone and is obtained using this equation:

$$R_{cond,cil} = \frac{\ln\left(r_{ext/int}\right)}{2\pi k_{perlite} cyl}. \quad (20)$$

(v) $R_{cond,uni}$ is the thermal resistance in the support zones and can be approximated with this equation:

$$\frac{1}{R_{cond,uni}} = \sum_{i=1}^{n} \frac{A_{trans,i} k_{steel}}{l_i}. \quad (21)$$

In this case the supports are simplified as sheets with a length l and an average transversal area. k_{steel} [7] will be obtained in the same way as perlite.

Now, the thermal circuit can be solved for the perlite in each load case. There is a problem because the radiation depends on the temperature of the exterior part of the tanker (12), so there is a fourth-order equation. It has been used MATLAB to solve the equations system using the Newton method. Table 2 shows the obtained results.

5.2. Calculation of the Superinsulation System. Two different insulation configurations have been analyzed, as showed in Figure 7.

5.3. Calculation of the Insulation Using Superinsulation in the Exterior. This is the configuration where the superinsulation is located between the parts of the tanker and joined only to the exterior part. It can be approximated with the equivalent circuit (Figure 8).

After establishing the equivalent circuit, the diverse variables involved must be defined. Some of them were defined for the perlite equivalent circuit.

(i) I_1 is the thermal power due to the diverse radiation emissions and can be obtained using (17).

(ii) $R_{cond,esp}$ is the thermal resistance due to the conduction in the diverse spherical zones, and it is obtained

Table 2: Analytical results obtained for the perlite.

Environmental temperature (°C)	Solar radiation (W/m^2)	Wind velocity (km/h)	T_{cext} (°C)	I (W)	Q_{abs} (W)
−10	0	0	−273.00	−1699.46	283.43
−10	0	100	−273.00	−2149.20	287.90
−10	0	200	−273.00	−2070.48	287.13
−10	500	0	−273.00	2819.65	294.74
−10	500	100	−273.00	3419.15	289.04
−10	500	200	−273.00	3446.71	288.77
−10	1000	0	−273.00	7266.10	305.84
−10	1000	100	−273.00	8986.54	290.17
−10	1000	200	−273.00	9064.86	289.42
0	0	0	−273.00	−1927.84	298.59
0	0	100	−273.00	−2490.19	303.60
0	0	200	−273.00	−2517.20	303.84
0	500	0	−273.00	2492.49	309.62
0	500	100	−273.00	3066.25	304.72
0	500	200	−273.00	3093.44	304.48
0	1000	0	−273.00	6835.27	320.48
0	1000	100	−273.00	8632.65	305.74
0	1000	200	−273.00	8703.74	305.13
20	0	0	−273.00	−2431.89	328.77
20	0	100	−273.00	−3285.49	334.95
20	0	200	−273.00	−3330.00	335.26
20	500	0	−273.00	1779.24	339.28
20	500	100	−273.00	2240.82	336.07
20	500	200	−273.00	2263.20	335.91
20	1000	0	−273.00	5913.48	349.62
20	1000	100	−273.00	7765.97	337.19
20	1000	200	−273.00	7856.01	336.55
50	0	0	−273.00	−3303.32	373.75
50	0	100	−273.00	−4807.02	381.91
50	0	200	−273.00	−4893.08	382.37
50	500	0	−273.00	638.90	383.17
50	500	100	−273.00	668.85	383.02
50	500	200	−273.00	671.84	383.00
50	1000	0	−273.00	4392.90	393.04
50	1000	100	−273.00	6143.35	384.12
50	1000	200	−273.00	6233.61	383.65

as the addition of the resistance at each layer (see Figure 8 and (22)):

$$R_{\text{cond,esp}} = \sum_{\text{SI}=1}^{3} R_{\text{cond,esp},i} + \sum_{\text{Lana}=1}^{2} R_{\text{cond,esp,lana}},$$
$$R_{\text{cond,esp,mat}} = \frac{1/r_{\text{int,mat}} - 1/r_{\text{ext,mat}}}{4\pi k_{\text{mat}}}, \tag{22}$$

where k_{mat} is the conductivity for each material at an average temperature.

(iii) $R_{\text{cond,cyl}}$ is the thermal resistance due to the conduction in the diverse cylindrical zones, and it is obtained as the addition of the resistance at each layer as follows (see equivalent circuit of Figure 9):

$$R_{\text{cond,cil}} = \sum_{\text{si}=1}^{3} R_{\text{cond,cyl,mat}} + \sum_{\text{lana}=1}^{2} R_{\text{conf,cyl,lana}},$$
$$R_{\text{cond,cyl,mat}} = \frac{\ln\left(r_{\text{ext,mat}}/r_{\text{int,mat}}\right)}{2\pi k_{\text{mat}} l_{\text{cyl}}}, \tag{23}$$

(iv) I_2 and I_3 are the heat fluxes due to the radiation inside the tanker, for the spherical and for the cylindrical

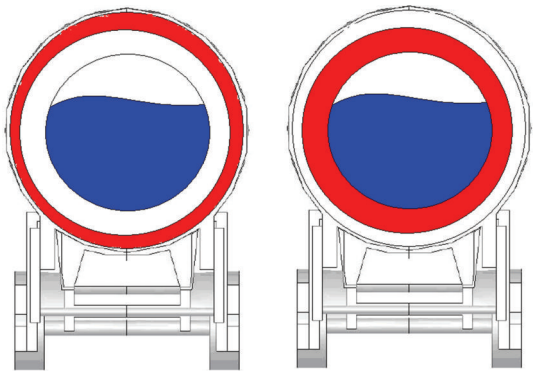

Figure 7: Insulation with vacuum and superinsulation in the exterior (left) and in the interior (right) parts of the tanker.

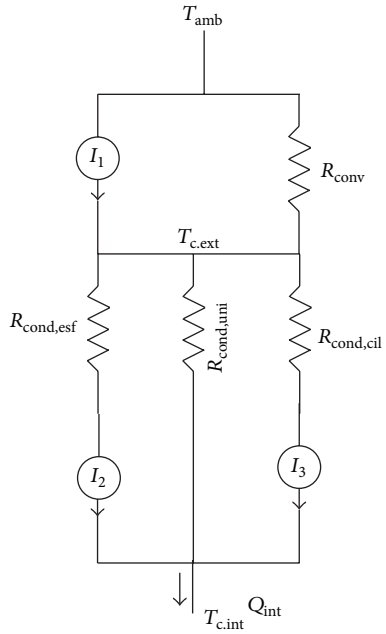

Figure 8: Equivalent circuit for the vacuum and superinsulation joined to the exterior part.

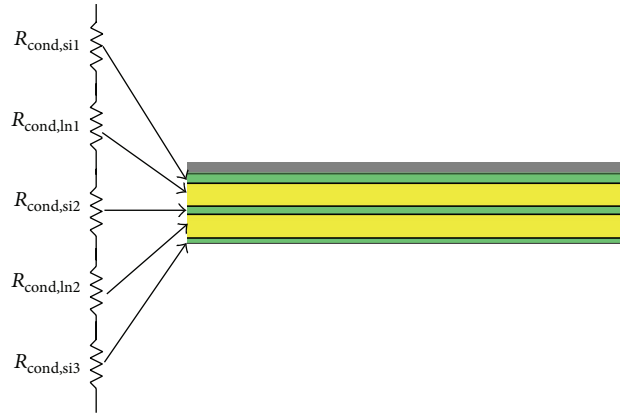

Figure 9: Equivalent conduction for the multilayer and the rock wool.

zone. They can be obtained using (14), and these final equations are obtained as follows:

$$\begin{aligned} I_2 &= A_{esp,int} q''_{rad,int} \\ &= 4\pi R_{int}^2 \left\{ \varepsilon_{int}\sigma T_{int}^4 \right. \\ &\quad - \varepsilon_{int}\sigma T_{int}^4 \alpha_{int} \sum_{i=0}^{\infty} \left[(1-\alpha_{ext})^{i+1} (1-\alpha_{int})^i \right] \\ &\quad \left. - \varepsilon_{ext}\sigma T_{ext}^4 \alpha_{ext} \frac{A_{int}}{A_{ext}} \sum_{i=0}^{\infty} \left[(1-\alpha_{ext})^i (1-\alpha_{int})^i \right] \right\}, \\ I_3 &= A_{cil,int} q''_{rad,ext} \\ &= 2\pi R_{int} \\ &\quad \times l_{int} \left\{ \varepsilon_{int}\sigma T_{int}^4 - \varepsilon_{int}\sigma T_{int}^4 \alpha_{int} \right. \\ &\quad \times \sum_{i=0}^{\infty} \left[(1-\alpha_{ext})^{i+1} (1-\alpha_{int})^i \right] \\ &\quad - \varepsilon_{ext}\sigma T_{ext}^4 \alpha_{ext} \frac{A_{int}}{A_{ext}} \\ &\quad \left. \times \sum_{i=0}^{\infty} \left[(1-\alpha_{ext})^i (1-\alpha_{int})^i \right] \right\}. \end{aligned} \tag{24}$$

Now, the equivalent circuit can be solved as in the perlite case. Table 5 shows the obtained results.

5.4. Calculation of the Insulation Using Superinsulation in the Interior. This is the configuration with the superinsulation located between the parts of the tanker and joined only to the interior part. It can be approximated with the equivalent circuit (Figure 10).

In this case, equations are similar to that obtained for the perlite and for the other superinsulation configuration; only I_2 and I_3 change as well as the k_{mat} value as follows:

$$\begin{aligned} I_2 &= A_{esf,ext} q''_{rad,ext} \\ &= 4\pi R_{ext}^2 \left\{ \varepsilon_{ext}\sigma T_{ext}^4 - \varepsilon_{ext}\sigma T_{ext}^4 \alpha_{ext} \right. \\ &\quad \times \sum_{i=0}^{\infty} \left[(1-\alpha_{int})^{i+1} (1-\alpha_{ext})^i \right] \\ &\quad - \varepsilon_{int}\sigma T_{int}^4 \alpha_{int} \frac{A_{int}}{A_{ext}} \\ &\quad \left. \times \sum_{i=0}^{\infty} \left[(1-\alpha_{ext})^i (1-\alpha_{int})^i \right] \right\}, \end{aligned}$$

$$
\begin{aligned}
I_3 &= A_{\text{cil,ext}} q''_{\text{rad,ext}} \\
&= 2\pi R_{\text{ext}} l_{\text{int}} \\
&\quad \times \left\{ \varepsilon_{\text{ext}} \sigma T_{\text{ext}}^4 - \varepsilon_{\text{ext}} \sigma T_{\text{ext}}^4 \alpha_{\text{ext}} \right. \\
&\qquad \times \sum_{i=0}^{\infty} \left[(1-\alpha_{\text{int}})^{i+1} (1-\alpha_{\text{ext}})^{i} \right] \\
&\qquad - \varepsilon_{\text{int}} \sigma T_{\text{int}}^4 \alpha_{\text{int}} \frac{A_{\text{int}}}{A_{\text{ext}}} \\
&\qquad \left. \times \sum_{i=0}^{\infty} \left[(1-\alpha_{\text{ext}})^{i} (1-\alpha_{\text{int}})^{i} \right] \right\}.
\end{aligned}
\tag{25}
$$

Now, the equivalent circuit can be solved as in the previous configurations. Table 6 shows the obtained results.

5.5. Insulation with Superinsulation and Perlite. A mixed insulation using superinsulation and perlite has a great disadvantage, which is the vacuum level needed. Although the required vacuum level is similar to the superinsulation vacuum level, this value is not compatible with perlite.

If we analyse Tables 3 and 4, it can be observed that with a 0.03 torr vacuum level, the superinsulation has a behaviour similar to the perlite's behaviour, so a mixed isolation has no sense because it has the same behaviour as perlite, but it is more expensive. Figure 10 shows the equivalent electric circuit.

5.6. Conclusions. After analysing the obtained results, it can be observed that the best configuration is the configuration with perlite, although the configuration with superinsulation in the exterior part also shows a good behavior. Analysing both in depth, it can be concluded that the perlite configuration has on average 2.2% better insulation capabilities, and that the maximum is 6.65% better if all load case for superinsulation in the exterior and perlite configurations are compared.

Concerning the configuration with superinsulation in the interior part, it can be observed that it is on average 65.8% worse and a maximum 85.7% worse. After analysing (14), it is observed that this behaviour is due to the fact that the radiation level depends on the temperature. Then, the configuration with the insulation in the exterior has lower temperature values than the configuration with the insulation in the interior (in this case the temperature is similar to the environmental temperature). In (14) the exterior temperature will govern the equations, whereas the interior temperature effect (between the radiation parts) is insignificant. In the radiation equations, temperature has a fourth-order, which implies a high heat absorption/emission difference.

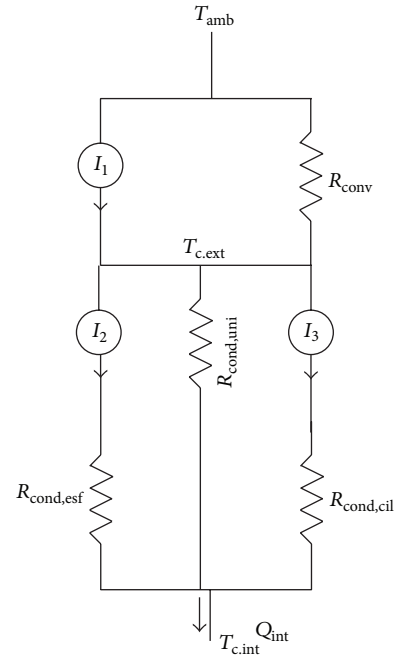

Figure 10: Equivalent circuit for the vacuum and superinsulation joined to the interior.

6. Numerical Simulation

Finite-elements method allows solving different kind of problems without an analytical solution; in this case it allows obtaining the real behaviour at any point of the tanker. On the one hand, this was a problem for an analytical solution. On the other hand, it does not require to simplify the problem (like in the analytical method), so results will be more similar to the real behaviour.

For this case, an axisymmetric model has been used because it allows to simplify the model and reduces the numerical requirements and the complexity of the mesh. Although this implies that exists an axis symmetry, which do not exist because the radiation load is not symmetric, load can be redistributed in all the exterior part to simplify the problem. A 3D model can be used to obtain the results with a higher accuracy level.

The main advantages of using an axisymmetric model instead of an analytical model are as follows.

(i) The effects of the supports are included.

(ii) Temperature values and the heat flux can be obtained at any point of the model.

(iii) It includes material properties dependent on the temperature and not with an average value.

(iv) The caps has their real geometry and not an approximated spherical geometry.

(v) The radiation can be obtained exactly, taking into account the real shape of the involved geometries, the supports, and so forth.

Table 3: Analytical results for insulation with the superinsulation joined to the exterior part of the tanker.

Environmental temperature (°C)	Solar radiation (W/m^2)	Wind velocity (km/h)	$T_{superins}$ (°C)	T_{cext} (°C)	I (W)	Q_{abs} (w)
−10	0	0	−273.00	−273.00	−3139.72	298.74
−10	0	100	−273.00	−273.00	−2292.25	289.30
−10	0	200	−273.00	−273.00	−2253.08	288.92
−10	500	0	−273.00	−273.00	1292.25	308.31
−10	500	100	−273.00	−273.00	3274.10	290.44
−10	500	200	−273.00	−273.00	3368.89	289.53
−10	1000	0	−273.00	−273.00	5659.65	319.07
−10	1000	100	−273.00	−273.00	8847.18	291.51
−10	1000	200	−273.00	−273.00	8982.58	290.21
0	0	0	−273.00	−273.00	−3769.34	314.39
0	0	100	−273.00	−273.00	−2669.87	305.17
0	0	200	−273.00	−273.00	−2633.56	304.85
0	500	0	−273.00	−273.00	559.19	325.02
0	500	100	−273.00	−273.00	2877.75	306.35
0	500	200	−273.00	−273.00	2987.54	305.40
0	1000	0	−273.00	−273.00	4802.64	335.56
0	1000	100	−273.00	−273.00	8433.18	307.45
0	1000	200	−273.00	−273.00	8599.17	306.03
20	0	0	−273.00	−273.00	−5329.45	348.80
20	0	100	−273.00	−273.00	−3586.55	337.07
20	0	200	−273.00	−273.00	−3502.61	336.48
20	500	0	−273.00	−273.00	−1247.53	358.87
20	500	100	−273.00	−273.00	1941.16	338.16
20	500	200	−273.00	−273.00	2170.14	336.56
20	1000	0	−273.00	−273.00	2790.96	368.60
20	1000	100	−273.00	−273.00	7455.17	339.34
20	1000	200	−273.00	−273.00	7686.43	337.74
50	0	0	−273.00	−273.00	−8625.47	401.04
50	0	100	−273.00	−273.00	−5413.26	385.09
50	0	200	−273.00	−273.00	−5237.08	384.18
50	500	0	−273.00	−273.00	−4920.08	410.19
50	500	100	−273.00	−273.00	58.39	386.20
50	500	200	−273.00	−273.00	324.44	384.82
50	1000	0	−273.00	−273.00	−1260.98	419.09
50	1000	100	−273.00	−273.00	5528.24	387.31
50	1000	200	−273	−273	5885.344591	385.462819

Figure 11 shows the FE mesh used for each insulation model.

The main aspect to make a good FEM simulation of a real problem is the correct establishment of the boundary conditions and the behaviour of the material; in this case diverse heat phenomena must be considered: convection, radiation, and conduction.

For this problem the software ABAQUS 6.10.2 has been used.

6.1. Conduction. Conduction is not difficult to simulate using numerical tools. It has been included the material with its properties dependent on the temperature (conductivity, specific heat).

6.2. Convection. Numerical programs like ABAQUS allow to simulate the convection phenomenon; in this case the parameter required is the convection coefficient (h_c), which must be obtained using convection equations. It can also be introduced depending on the temperature, using curves and fields.

6.3. Radiation. It is a quite difficult to simulate the radiation phenomenon with numerical tools; in this case there are four different types of radiation: solar radiation, environmental radiation, the radiation of the exterior part to the environment, and the radiation inside the tanker in the superinsulation configuration.

Table 4: Analytical results for insulation with the superinsulation in the interior of the tanker.

Environmental temperature (°C)	Solar radiation (W/m^2)	Wind velocity (km/h)	$T_{superins}$ (°C)	T_{cext} (°C)	I (W)	Q_{abs} (w)
−10	0	0	−273.00	−273.00	−1648.15	529.46
−10	0	100	−273.00	−273.00	−2144.70	529.25
−10	0	200	−273.00	−273.00	−2168.53	529.74
−10	500	0	−273.00	−273.00	2878.53	533.93
−10	500	100	−273.00	−273.00	3424.34	541.95
−10	500	200	−273.00	−273.00	3449.14	493.26
−10	1000	0	−273.00	−273.00	7326.31	522.36
−10	1000	100	−273.00	−273.00	8991.94	529.94
−10	1000	200	−273.00	−273.00	9067.30	525.40
0	0	0	−273.00	−273.00	−1874.08	526.84
0	0	100	−273.00	−273.00	−2484.79	510.82
0	0	200	−273.00	−273.00	−2514.50	520.11
0	500	0	−273.00	−273.00	2548.68	521.73
0	500	100	−273.00	−273.00	3070.79	517.79
0	500	200	−273.00	−273.00	3095.97	530.91
0	1000	0	−273.00	−273.00	6899.80	533.13
0	1000	100	−273.00	−273.00	8625.34	523.73
0	1000	200	−273.00	−273.00	8705.92	527.56
20	0	0	−273.00	−273.00	−2371.78	537.55
20	0	100	−273.00	−273.00	−3279.94	520.47
20	0	200	−273.00	−273.00	−3326.43	529.21
20	500	0	−273.00	−273.00	1840.88	529.99
20	500	100	−273.00	−273.00	2246.41	536.92
20	500	200	−273.00	−273.00	2267.00	550.16
20	1000	0	−273.00	−273.00	5991.50	567.49
20	1000	100	−273.00	−273.00	7771.61	552.21
20	1000	200	−273.00	−273.00	7859.82	556.88
50	0	0	−273.00	−273.00	−3235.41	552.79
50	0	100	−273.00	−273.00	−4798.10	573.79
50	0	200	−273.00	−273.00	−4885.92	571.59
50	500	0	−273.00	−273.00	662.86	570.70
50	500	100	−273.00	−273.00	676.03	568.91
50	500	200	−273.00	−273.00	676.93	575.49
50	1000	0	−273.00	−273.00	4494.30	597.32
50	1000	100	−273.00	−273.00	6149.68	586.82
50	1000	200	−273.00	−273.00	6239.62	592.86

Solar and environmental radiation can be simulated as a heat flux using (11) and (12). Radiation of the exterior part to the environment can be simulated like a heat flux dependent on the temperature of the external part at each point, using the ABAQUS command RADIATE; this command uses the emissivity of steel, and radiation can be obtained depending on the temperature at each point, instead of using an average value like in the analytical model.

The most difficult radiation type to simulate is the interior radiation. It has been also simulated using the command RADIATE at each point of the diverse surfaces, but considering that the real geometry and each cavity could absorb and reflect it. Therefore it has been simulated each cavity (10: 2 cylinders, 4 caps, and 4 supports), and the ray theory has been used. The Steffan-Boltzman theory has been applied to analyse the radiation between these cavities. Equation (26) defines this radiation [6]:

$$q_i^c = \frac{\sigma \varepsilon_i}{A_i} \sum \varepsilon_j \sum F_{ik} C_{kj}^{-1} \left[\left(\theta_j - \theta_z\right)^4 - \left(\theta_i - \theta_z\right)^4 \right], \quad (26)$$

where A_i is the area of each face in each element of the i cavity, ε_i, ε_j are the emissivity of the face i or of the face j, F_{ik} is the shape factors matrix of the face i, C_{ij} is the reflection matrix between the face i and the j, θ_i, θ_j are the temperature (°K) of the face i or j, and θ_z is the zero temperature.

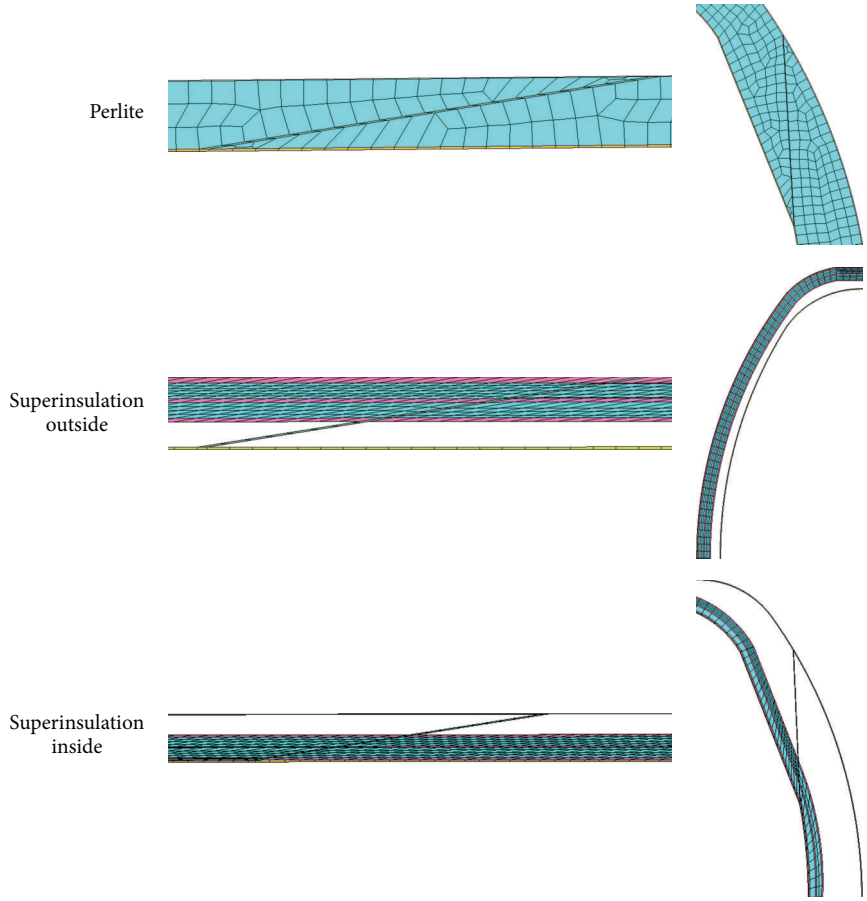

Figure 11: Detail of the support zones for each FEM model.

This equation is equivalent to (14) equation but with a matrix expression.

The shape factors matrix is automatically obtained with the numerical software, but it is necessary to define the block grade; in this case a partial grade has been used because it allows the reflection between surfaces. By this way the software is able to obtain the successive radiations and absorptions.

6.4. Boundaries. There is only one boundary condition to apply to the numerical model which is the temperature of the liquid contained. For this case the liquid temperature is −193°C, and this value has been applied to the inner face of the interior part of the tanker.

6.5. Obtained Results. See Figure 12.

6.6. Conclusions. After analysing the results (see Table 7), it can be observed that whereas the best insulation results are obtained for the perlite configuration, the configuration with superinsulation in the interior provides the worst.

Analysing the temperatures, it can be observed that temperatures in the steel parts of the tanker do not show important variations and that the effect of convection has not a high influence on results.

It can be observed that numerical results have lower heat flux values (due to the fact of the blocking of the radiation, to the effects of temperature on the material properties, and to the simulation of the real geometry of the caps) and therefore show better performance than analytical results (see Table 7).

The maximum error between the numerical and the analytical results is 23.9%, and the average error is 7.8%. A higher heat flux for the analytical method implies that the analytical method can be used with a high accuracy level.

It can be observed that there is a high heat flux through the supports, because they are made of steel, which has a high thermal conductivity, so to reduce these heat losses, a heat bridge should be used.

7. Exterior Finish Thermal Behaviour

The influence of the exterior finish of the tanker on the heat fluxes and on the exterior temperature has been analysed for each load case in the perlite insulation configuration.

Figure 13 shows the approximated absorption and emission factor values (emissivity or absorptivity/10).

Using (11), it can be observed that the best behaviour will be achieved with a high emissivity and a low absorptivity. Those materials showing this behaviour are called selective cooling materials, and they present high energy emission

Table 5: Comparative table (exterior temperature and heat flux) for the analytical and the numerical results.

Environmental temperature (°C)	Solar radiation (W/m^2)	Wind velocity (km/h)	Perlite				Superinsulation outside				Superinsulation inside			
			Numerical		Analytical		Numerical		Analytical		Numerical		Analytical	
			T_{cext} (°C)	Q_{abs} (W)	T_{cext} (°C)	Q_{abs} (W)	T_{cext} (°C)	Q_{abs} (W)	T_{cext} (°C)	Q_{abs} (W)	T_{cext} (°C)	Q_{abs} (W)	T_{cext} (°C)	Q_{abs} (W)
−10	0	0	−10.70	242.70	−13.16	283.43	−11.00	269.40	−4.37	298.74	−10.00	511.40	−13.49	529.46
−10	0	100	−10.10	248.00	−10.32	287.90	−10.00	267.30	−9.44	289.30	−10.00	509.40	−10.35	529.25
−10	0	200	−10.00	248.70	−10.81	287.13	−10.00	267.50	−9.68	288.92	−10.00	510.30	−10.20	529.74
−10	500	0	−9.50	244.80	−5.98	294.74	−10.00	269.20	2.63	308.31	−10.00	514.30	−6.33	533.93
−10	500	100	−9.90	248.30	−9.60	289.04	−10.10	268.10	−8.71	290.44	−10.00	521.50	−9.63	541.95
−10	500	200	−10.00	248.80	−9.77	288.77	−10.00	267.90	−9.29	289.53	−10.00	506.30	−9.79	493.26
−10	1000	0	−8.30	246.90	1.06	305.84	−10.00	271.30	9.45	319.07	−10.10	499.20	0.73	522.36
−10	1000	100	−9.80	248.50	−8.88	290.17	−10.10	267.70	−8.03	291.51	−10.00	509.30	−8.91	529.94
−10	1000	200	−9.90	249.00	−9.36	289.42	−10.00	268.40	−8.86	290.21	−10.00	506.40	−9.38	525.40
0	0	0	−0.80	262.10	−3.54	298.59	−0.10	274.30	6.49	314.39	−0.10	507.10	−3.85	526.84
0	0	100	−0.10	267.80	−0.36	303.60	0.00	273.70	0.63	305.17	0.00	494.30	−0.39	510.82
0	0	200	−0.10	268.50	−0.21	303.84	0.00	273.50	0.43	304.85	0.00	504.10	−0.23	520.11
0	500	0	0.40	264.10	3.46	309.62	0.00	275.10	13.23	325.02	−0.10	505.20	3.16	521.73
0	500	100	0.10	268.00	0.35	304.72	−0.10	274.00	1.38	306.35	0.00	503.10	0.32	517.79
0	500	200	0.00	268.60	0.20	304.48	0.00	274.30	0.78	305.40	0.00	514.50	0.19	530.91
0	1000	0	1.50	266.10	10.35	320.48	0.00	275.80	19.92	335.56	−0.10	517.60	10.03	533.13
0	1000	100	0.20	268.30	1.00	305.74	−0.10	274.70	2.09	307.45	0.00	508.40	1.04	523.73
0	1000	200	0.10	268.40	0.61	305.13	0.00	275.20	1.18	306.03	0.00	511.40	0.60	527.56
20	0	0	19.10	301.30	15.61	328.77	19.90	312.10	28.32	348.80	19.90	521.50	15.33	537.55
20	0	100	19.90	307.60	19.53	334.95	20.00	307.40	20.88	337.07	20.00	512.30	19.51	520.47
20	0	200	19.90	308.50	19.73	335.26	20.00	307.70	20.50	336.48	20.00	519.80	19.71	529.21
20	500	0	20.10	303.00	22.28	339.28	19.90	312.30	34.71	358.87	19.90	520.10	22.01	529.99
20	500	100	20.00	307.90	20.24	336.07	20.00	313.10	21.57	338.16	20.00	517.10	20.22	536.92
20	500	200	20.00	308.70	20.14	335.91	20.00	313.20	20.56	336.56	20.00	534.10	20.12	550.16
20	1000	0	21.20	304.90	28.84	349.62	19.90	312.60	40.89	368.60	19.90	545.30	28.52	567.49
20	1000	100	20.20	308.20	20.95	337.19	20.00	316.70	22.32	339.34	20.00	536.20	20.93	552.21
20	1000	200	21.70	305.80	20.55	336.55	20.00	313.40	21.30	337.74	20.00	540.10	20.53	556.88
50	0	0	48.80	367.30	44.15	373.75	49.90	380.30	61.47	401.04	49.90	538.70	43.91	552.79
50	0	100	49.80	375.90	49.33	381.91	50.00	378.70	51.35	385.09	50.00	555.10	49.30	573.79
50	0	200	49.90	377.00	49.62	382.37	50.00	377.20	50.77	384.18	50.00	551.90	49.60	571.59
50	500	0	49.80	369.60	50.13	383.17	49.90	381.30	67.27	410.19	49.80	550.40	50.05	570.70
50	500	100	50.00	376.20	50.03	383.02	50.00	378.90	52.05	386.20	50.00	548.40	50.01	568.91
50	500	200	50.00	377.20	50.02	383.00	50.00	382.10	51.17	384.82	50.00	558.90	50.00	575.49
50	1000	0	50.70	371.60	56.39	393.04	49.90	403.10	72.92	419.09	49.80	574.70	56.07	597.32
50	1000	100	50.10	376.71	50.73	384.12	50.00	399.70	52.75	387.31	50.00	567.20	50.71	586.82
50	1000	200	50.10	377.73	50.43	383.65	50.00	401.20	51.58	385.46	50.00	570.20	50.41	592.86

Table 6: Heat fluxes for the perlite insulation configuration depending on the external surface properties.

Material (absorptivity, emissivity, and reflectivity)			Polish stainless steel	Stripped stainless steel	Galvanized steel	White painted steel	Black painted	Black laquer	Dark grey paint	Dark blue painted	Silver painted	White laquer	Aluminium paint	Shiny white paint	Minimum heat flux (W)
Environmental temperature (°C)	Solar radiation (W/m^2)	Wind velocity (km/h)	0.3 0.7 0.33	0.52 0.48 0.27	0.62 0.38 0.19	0.23 0.77 0.77	0.95 0.05 0.97	0.92 0.08 0.89	0.91 0.09 0.86	0.91 0.09 0.75	0.25 0.75 0.67	0.21 0.79 0.2	0.4 0.6 0.5	0.21 0.79 0.87	
−10	0	0	298.74	269.60	274.38	247.03	240.15	242.80	243.82	247.77	250.85	273.76	258.04	243.48	240.15
−10	0	100	289.30	286.60	287.12	283.54	282.35	282.82	283.00	283.65	284.14	287.06	285.17	282.94	282.35
−10	0	200	288.92	287.37	287.67	285.58	284.87	285.15	285.26	285.65	285.93	287.63	286.54	285.22	284.87
−10	500	0	308.31	290.15	299.91	254.53	268.48	270.90	271.88	276.81	259.91	282.43	272.27	250.12	250.12
−10	500	100	290.44	288.57	289.48	284.38	285.80	286.18	286.33	287.00	285.13	287.85	286.67	283.71	283.71
−10	500	200	289.53	288.50	289.02	286.07	286.89	287.11	287.20	287.59	286.51	288.09	287.40	285.67	285.67
−10	1000	0	319.07	310.19	324.82	261.88	294.60	296.91	297.89	303.81	268.80	291.02	286.12	256.65	256.65
−10	1000	100	291.51	290.54	291.83	285.23	289.25	289.53	289.65	290.34	286.13	288.65	288.16	284.48	284.48
−10	1000	200	290.21	289.63	290.37	286.56	288.90	289.06	289.13	289.53	287.09	288.55	288.26	286.12	286.12
0	0	0	314.39	282.78	288.17	257.84	250.35	253.22	254.34	258.65	262.01	287.47	269.91	253.96	250.35
0	0	100	305.17	302.09	302.68	298.55	297.19	297.73	297.93	298.68	299.24	302.61	300.43	297.86	297.19
0	0	200	304.85	302.97	303.32	300.90	300.09	300.41	300.53	300.98	301.31	303.27	302.01	300.49	300.09
0	500	0	325.02	303.01	313.37	265.13	277.88	280.55	281.63	286.92	270.85	296.03	283.83	260.43	260.43
0	500	100	306.35	304.05	305.03	299.39	300.62	301.07	301.24	302.01	300.23	303.40	301.92	298.63	298.63
0	500	200	305.40	304.10	304.66	301.38	302.09	302.36	302.46	302.91	301.88	303.73	302.87	300.93	300.93
0	1000	0	335.56	322.71	337.94	272.29	303.28	305.86	306.94	313.22	279.51	304.50	297.37	266.78	266.78
0	1000	100	307.45	306.01	307.39	300.23	304.04	304.40	304.54	305.34	301.22	304.20	303.41	299.39	299.39
0	1000	200	306.03	305.23	306.01	301.87	304.10	304.30	304.39	304.85	302.46	304.19	303.73	301.38	301.38
20	0	0	348.80	308.52	315.22	278.59	269.89	273.22	274.51	279.54	283.49	314.35	292.88	274.08	269.89
20	0	100	337.07	332.95	333.73	328.33	326.58	327.27	327.53	328.51	329.23	333.64	330.78	327.45	326.58
20	0	200	336.48	334.17	334.57	331.38	330.32	330.75	330.90	331.49	331.92	334.51	332.84	330.85	330.32
20	500	0	358.87	328.10	339.74	285.51	295.90	299.06	300.34	306.35	291.89	322.67	306.18	280.19	280.19
20	500	100	338.16	334.91	336.08	329.16	329.96	330.57	330.80	331.80	330.21	334.43	332.26	328.20	328.20
20	500	200	336.56	335.24	335.91	331.87	332.31	332.68	332.82	333.41	332.49	334.97	333.70	331.29	331.29
20	1000	0	368.60	347.07	363.61	292.29	319.95	323.04	324.33	331.32	300.12	330.91	319.11	286.20	286.20
20	1000	100	339.34	336.86	338.43	329.99	333.33	333.85	334.06	335.09	331.19	335.22	333.73	328.95	328.95
20	1000	200	337.74	336.36	337.26	332.36	334.30	334.61	334.73	335.34	333.07	335.42	334.55	331.73	331.73
50	0	0	401.04	345.60	354.42	307.72	297.19	301.20	302.77	308.88	313.72	353.25	325.41	302.24	297.19
50	0	100	385.09	378.90	380.12	372.34	369.86	370.84	371.21	372.59	373.61	379.98	375.84	371.09	369.86
50	0	200	384.18	380.67	381.33	376.70	375.18	375.78	376.01	376.85	377.47	381.25	378.81	375.93	375.18
50	500	0	410.19	364.10	377.89	314.11	321.14	325.03	326.59	333.67	321.50	361.21	337.81	307.87	307.87
50	500	100	386.20	380.93	382.45	373.15	373.16	374.06	374.41	375.82	374.58	380.77	377.30	371.82	371.82
50	500	200	384.82	381.79	382.67	377.18	377.14	377.69	377.90	378.76	378.04	381.70	379.66	376.37	376.37
50	1000	0	419.09	382.07	400.69	320.38	343.36	347.20	348.78	356.81	329.13	369.08	349.87	313.41	313.41
50	1000	100	387.31	382.86	384.79	373.97	376.46	377.28	377.60	379.05	375.55	381.56	378.76	372.56	372.56
50	1000	200	385.46	382.91	384.01	377.66	379.10	379.59	379.79	380.66	378.61	382.16	380.51	376.81	376.81

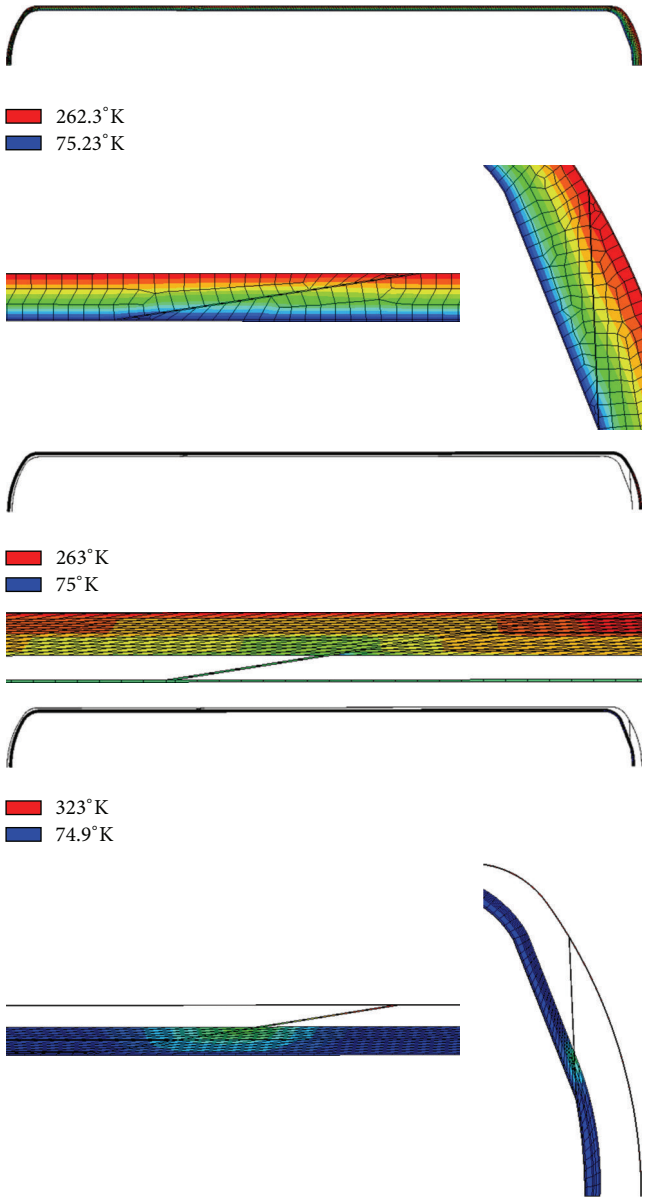

Figure 12: Temperature at each point for the configurations: perlite (top), superinsulation in the exterior (middle), and superinsulation in the interior part of the tanker (down).

and reflection capabilities. Some of these materials used for tankers are white paint, white lacquered, and white galvanized steel.

Analyzing Table 7, the desirable properties are indicated in bold letters. With these values, the results of Table 6 are obtained. Analyzing the results, we can see that, without solar radiation, the best surface finish is the black paint, because it has the highest emissivity coefficient, and in this case the heat emission is higher than the absorption.

On the other hand, with solar emissions the incident solar radiation is the main heat source, so in this case it will better the surface finish with the best absorptivity and the lower emissivity.

Table 7: Thermal properties depending on the surface finish for tankers [11].

	Absorptivity	Reflectivity	Emissivity
Polish stainless steel	**0.3**	0.7	0.33
Stripped stainless steel	0.52	0.48	0.27
Galvanized steel	0.62	0.38	0.19
White painted steel	**0.23**	0.77	0.77
Black painted	0.95	0.05	**0.97**
Black laquer	0.92	0.08	**0.89**
Dark grey paint	0.91	0.09	**0.86**
Dark blue painted	0.91	0.09	**0.75**
Silver painted	**0.25**	0.75	**0.67**
White laquer	**0.21**	0.79	0.2
Aluminium paint	**0.4**	0.6	0.5
Shiny white paint	**0.21**	0.79	**0.87**

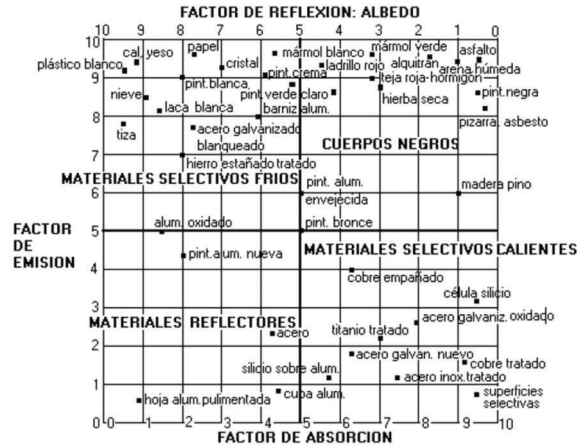

Figure 13: Reflection and emission factor for some different surface finish [12].

8. Maximum Transport Time for Tanker

To obtain the maximum time to transport the liquid, the first step is to understand the process that takes place inside the tanker. Inside the interior part of the tanker there is a fluid that using cold temperatures and pressure has been changed from a gas state into a liquid + gas state. The quantity of liquid depends on the filling level and is lower than the 100%, because it must be a gas inside the tanker to make a pressure, so there must be a gas-liquid equilibrium. A common filling level is 98%.

There must not exist another gas inside the tanker, because it would mix with the liquid to transport, and the degree of purity of this liquid would be modified, so other gases are removed during the filling operation.

So, in order to make the calculation, the Clausius-Clapeyron diagrams of these gases are needed to obtain the initial and final filling levels, pressures, temperatures, and so forth.

These graphics also show the process that takes place inside the tanker; this is a constant volume heating.

Then the liquid tends to head, the gas amount increases due to the liquid evaporation, and this increases the internal pressure; internal pressures and temperatures are directly involved.

To obtain the heat flux, it is necessary to carry out an energy balance between the initial and the final state. Equation (27) shows this energy balance:

$$\begin{aligned}
&m_{\text{final,gas}} \cdot h_{\text{gas}}\left(P_{\text{final}} V_{\text{total}}\right) \\
&\quad + m_{\text{final,liquid}} \cdot h_{\text{liquid}}\left(P_{\text{final}} V_{\text{total}}\right) \\
&= \dot{Q}\Delta T + m_{\text{initial,gas}} \cdot h_{\text{gas}}\left(P_{\text{initial}} V_{\text{total}}\right) \\
&\quad + m_{\text{inicial,liquid}} \cdot h_{\text{liquid}}\left(P_{\text{initial}} V_{\text{total}}\right) \\
&\longrightarrow \dot{Q}\Delta T = m_{\text{final,gas}} \cdot h_{\text{gas}}\left(P_{\text{final}} V_{\text{total}}\right) \\
&\quad + m_{\text{final,liquid}} \cdot h_{\text{liquid}}\left(P_{\text{final}} V_{\text{total}}\right) \\
&\quad - m_{\text{initial,gas}} \cdot h_{\text{gas}}\left(P_{\text{initial}} V_{\text{total}}\right) \\
&\quad - m_{\text{initial,liquid}} \cdot h_{\text{liquid}}\left(P_{\text{initial}} V_{\text{total}}\right) \\
&= \frac{100 - \text{GL}_{\text{final}}}{100} \cdot V_{\text{total}} \cdot \rho_{\text{gas,final}} \\
&\quad \cdot h_{\text{gas}}\left(P_{\text{final}} V_{\text{total}}\right) \\
&\quad + \frac{\text{GL}_{\text{final}}}{100} \cdot V_{\text{total}} \cdot \rho_{\text{liquid,final}} \\
&\quad \cdot \rho_{\text{liquid,final}} \cdot h_{\text{gas}}\left(P_{\text{final}} V_{\text{total}}\right) \\
&\quad - \frac{100 - \text{GL}_{\text{inicial}}}{100} \cdot V_{\text{total}} \\
&\quad \cdot \rho_{\text{gas,initial}} \cdot h_{\text{gas}}\left(P_{\text{initial}} V_{\text{total}}\right) \\
&\quad - \frac{\text{GL}_{\text{initial}}}{100} \cdot V_{\text{total}} \cdot \rho_{\text{liquid,initial}} \\
&\quad \cdot \rho_{\text{liquid,initial}} \cdot h_{\text{gas}}\left(P_{\text{initial}} V_{\text{total}}\right),
\end{aligned} \tag{27}$$

where Δt is the maximum time to perform the transport, P_{final} is the maximum pressure that could be reached before the safety valve acts, and the gas is evacuated to the environment.

Now the problem can be solved, so the time can be obtained.

To obtain the initial filling level, we use the properties of the gas and the saturation pressure for each temperature. With a mass balance, (28) is obtained:

$$\begin{aligned}
m_{\text{inicial}} &= m_{\text{inicial,gas}} + m_{\text{inicial,liquid}} \\
&= m_{\text{final}} = m_{\text{final,gas}} + m_{\text{final,liquid}} \\
&= \frac{\text{GL}_{\text{inicial}}}{100} V_{\text{total}} \cdot \rho_{\text{liquid,init}} \\
&\quad + \frac{100 - \text{GL}_{\text{initial}}}{100} V_{\text{total}} \cdot \rho_{\text{gas,init}} \\
&= \frac{\text{GL}_{\text{final}}}{100} V_{\text{total}} \cdot \rho_{\text{liquid,final}} \\
&\quad + \frac{100 - \text{GL}_{\text{final}}}{100} V_{\text{total}} \cdot \rho_{\text{gas,final}} \\
&\longrightarrow \frac{\text{GL}_{\text{inicial}}}{100} \cdot \rho_{\text{liquid,initial}} \\
&\quad + \frac{100 - \text{GL}_{\text{initial}}}{100} \cdot \rho_{\text{gas,initial}} \\
&= \frac{\text{GL}_{\text{final}}}{100} \cdot \rho_{\text{liquid,final}} + \frac{100 - \text{GL}_{\text{final}}}{100} \cdot \rho_{\text{gas,final}}.
\end{aligned} \tag{28}$$

Now, the filling level can be obtained for any temperature, depending on the filling level at a specific temperature.

The following equation must be fulfilled too:

$$\text{GL}(T) \leq \text{GL}_{\max} \text{para} \, T \in \left[T_{\min}, T_{\max}\right]. \tag{29}$$

Therefore, solving (27), (28), and (29), the initial filling level, the mass, temperatures, and initial pressures can be obtained, and by this way, the maximum transport time can be calculated for each insulation configuration.

In this particular case, the maximum filling level is 98% with a maximum and minimum pressures of 5.5 and 1 atm, respectively. Using (28), we obtain an initial filling level of 87.3% for nitrogen. Using (27), we obtain

$$\dot{Q}\Delta t = 1.143 \cdot 10^{9} \, \text{J}. \tag{30}$$

If data obtained in Table 8 is used, the maximum transport distance and time can be calculated (see Table 8).

Although time values that appears in Table 8 seem too high, they are inside the ranges that builders of this type of vehicles use to have experimentally. This time value indicates the maximum time that you could have the gas inside, before the pressure emergency valve acts; however, the time is usually lower. On the other hand, a high time value indicates that the final temperature of the liquid will be lower and so if this liquid would be stored later in a cryogenic tanker, the energy needed to cool it would be lower.

9. Analysis of the Frost outside the Tanker

Another phenomenon that has to be considered is the frost that can appear in the exterior part of the tanker. This frost shows a bad visual aspect and therefore should be taken into account during the design stage. This frost appears because the exterior tanker has a temperature lower than the environmental one: if it is lower than the fusion temperature of water (0°C), frost appears. On the contrary, if it is higher, water condensation usually appears due to the condensation of the air humidity.

Equation (31) shows the temperature value, depending on the environmental temperature and the humidity, below which the condensation appears. This temperature is called dew temperature [6].

Table 8: Maximum transportation time (in days).

Environmental temperature (°C)	Solar radiation (W/m^2)	Wind velocity (km/h)	Perlite	Superinsulation outside	Superinsulation inside
−10	0	0	41.25	39.13	22.08
−10	0	100	40.61	40.41	22.09
−10	0	200	40.72	40.46	22.07
−10	500	0	39.66	37.92	21.90
−10	500	100	40.45	40.25	21.57
−10	500	200	40.49	40.38	23.70
−10	1000	0	38.23	36.64	22.38
−10	1000	100	40.29	40.10	22.06
−10	1000	200	40.39	40.28	22.25
0	0	0	39.15	37.19	22.19
0	0	100	38.51	38.31	22.89
0	0	200	38.48	38.35	22.48
0	500	0	37.76	35.97	22.41
0	500	100	38.37	38.16	22.58
0	500	200	38.40	38.28	22.02
0	1000	0	36.48	34.84	21.93
0	1000	100	38.24	38.02	22.32
0	1000	200	38.31	38.20	22.16
20	0	0	35.56	33.52	21.75
20	0	100	34.90	34.68	22.46
20	0	200	34.87	34.74	22.09
20	500	0	34.46	32.58	22.06
20	500	100	34.79	34.57	21.77
20	500	200	34.80	34.74	21.25
20	1000	0	33.44	31.72	20.60
20	1000	100	34.67	34.45	21.17
20	1000	200	34.74	34.62	20.99
50	0	0	31.28	29.15	21.15
50	0	100	30.61	30.36	20.37
50	0	200	30.58	30.43	20.45
50	500	0	30.51	28.50	20.49
50	500	100	30.52	30.27	20.55
50	500	200	30.52	30.38	20.31
50	1000	0	29.74	27.90	19.57
50	1000	100	30.44	30.19	19.92
50	1000	200	30.47	30.33	19.72

Consider

$$T_{\text{dew}} = \sqrt[8]{\frac{\text{humidity}}{100}} \cdot \left(112 + 0,9T_{\text{env}}\right) + 0,1T_{\text{env}} - 112. \quad (31)$$

Then, if the temperature at any point of the external surface of the tanker is lower than the dew temperature, condensation will appear, and if it is lower than 0°C, it will appear frost. These phenomena usually appear in the coldest temperature zones which are the support zones of the tanker, because there is a high conductivity, and therefore show a lower temperature.

10. Conclusions

The main conclusions that are obtained from this thermal analysis are, on the one hand, that the analytical approximation can solve the problem with a good accuracy level and with this method different insulation and vacuum levels can be compared. Moreover, analytical results are obtained quickly and without using numerical tools (which would

require a higher work and higher computational cost), and the exterior temperature and the heat flux can also be obtained.

The axisymmetric model allows a better solution of the problem, and with it, there can be obtained the temperatures and heat fluxes at any point and therefore the worse insulation locations and the temperature map of the tanker.

Another aspect analysed was the exterior finish of the tanker, because a good selection of this aspect entails lower heat fluxes and losses and, as a result of this, higher transportation times with a low manufacturing cost.

The best insulation configuration is the perlite one, although the superinsulation in the exterior part showed a similar behaviour with a more expensive cost. The superinsulation in the interior configuration showed the worst behaviour.

It can be observed that the superinsulation and the perlite properties depend on the vacuum level, and depending on this aspect the behaviour changes.

It has to be taken into account, when the isolation is selected, that when there is a vacuum loss (during an accident, a perforation, etc.), the perlite configuration has always a better behaviour because it is not very sensitive to temperature. The superinsulation has worse properties, because without vacuum, convention phenomena appear inside the tanker and heat losses increase a lot. In the case of the perlite configuration, although this implies a conductivity increase, quite lower heat losses appear, and therefore the perlite configuration allows containing the fluid inside the tanker for much more time.

Acknowledgments

The publication of this research paper has been possible thanks to the funding given by the Industry and Innovation Department of the Government of Aragon as well as by the European Social Funds to the Research Group VEHIVIAL, according to Regulation (CE) no. 1828/2006 of the 8 of December Commission.

References

[1] I. Bures, V. Chrz, S. Smrz et al., "Cryogenic tankers—designed for safety," in *Procceings of the 5th Cryogenics IIR International Conference*, Prague, Czech Republic, May 1998.

[2] L. R. Jamison and J. P. Johnson, "Cryogenic tanker operation in North-West Pacific," *Chemical Engineer-London*, no. 308, pp. 256–256, 1976.

[3] D. McCaslin, "Cryogenic rail tankers," *Cryogenics*, vol. 11, no. 4, pp. 268–26, 1971.

[4] J. Brac, P. Odru, and J. M. Gérez, "Flow and thermal modelling in cryogenic flexible pipe," in *Proceedings of the 12th International Offshore and Polar Engineering Conference (ISOPE '02)*, vol. 2, pp. 47–54, Kyushu, Japan, May 2002.

[5] Perlite Institute, http://www.perlite.org/.

[6] M. Muñoz and J. A. Rodríguez-Pomatta, *Transmisión del Calor*, Universidad Nacional de Educación a Distancia, Madrid, Spain, 2004.

[7] E. D. Marquardt, J. P. Le, and R. Radebaugh, "Cryogenic material properties database," in *Proceedings of the 11th International Cryocooler Conference*, Juny 2000.

[8] "Multilayer Inc base date," http://www.multilayer.com/.

[9] NBE-AE-82 Spanish regulation, "Acciones en la Edificación".

[10] L. Mei, D. G. Infield, R. Gottschalg, D. L. Loveday, D. Davies, and M. Berry, "Equilibrium thermal characteristics of a building integrated photovoltaic tiled roof," *Solar Energy*, vol. 83, no. 10, pp. 1893–1901, 2009.

[11] "Omega institute data base," http://www.omega.com/literature/.

[12] V. Musilova, P. Hanzelka, T. Kralik, and A. Srnka, "Low temperature radiative properties of materials used in cryogenics," *Cryogenics*, vol. 45, no. 8, pp. 529–536, 2005.